Some Aspects of the Flow of Stratified Fluids

III. Continuous Density Gradients

By ROBERT R. LONG, the Johns Hopkins University[1]

(Manuscript received April 5, 1955)

Abstract

The investigations of Parts I and II are extended to include experiments and theoretical considerations relating to the behavior of fluid systems with continuous gradients of density. The general equation of steady-state motion derived in Part I is integrated to yield the flow of a stratified fluid over an obstacle of finite dimensions. The results indicate a more or less complicated laminar wave motion for obstacles of maximum height below a certain value. Larger barriers cause an overdevelopment of the waves to a point where closed circulations and negative horizontal velocities appear. It is shown that this is accompanied by locally unstable distributions of density and eventual turbulence. If the height of the barrier is further increased, the velocity increases indefinitely in some parts of the field, becoming infinite for an obstacle of a certain size. No steady-state solution exists for larger barriers. The two critical values of the obstacle height depend primarily on the Froude number: If this number exceeds $1/\pi$ the solution exists and is stable for all obstacles; for small Froude numbers the barrier must be small if the solution is to exist or be stable.

If the obstacle is small enough to permit laminar or moderately turbulent motion, the accompanying experiments verify all important features of the theory with remarkable fidelity. Larger obstacles cause considerable turbulence and blocking effects which propagate upstream, causing alternate maxima (jets) and minima of horizontal velocity in the vertical.

1. Introduction

Part I of this series of papers (LONG 1953) contained a theoretical analysis of the steady-state flow of a stratified fluid over a barrier. Part II (LONG 1954) represented an attempt to investigate experimentally the simplest possible system of this type: the flow of two superimposed layers of different density over a smooth boundary of finite dimensions. In the latter investigation it was possible to present an accompanying theory which explained rather well the observed behavior. In general shock waves or internal hydraulic jumps in the lee of the barrier are the only phenomena of any great importance and these occurred as predicted by the theory.

In many applications of stratified theory to natural phenomena, it has been assumed that a fluid system with continuous density gradient may be approximated by layered systems (ABDULLAH 1954, TEPPER 1952). There is really no evidence to support such an assumption and it appeared to be desirable, for this and other reasons, to extend the theory and experiments to systems with continuous density stratification. It is the purpose of this paper to present the results of this investigation.

---

[1] This research was supported by the U.S. Weather Bureau. Presented at the 5th Congress of the OSTIV (Organisation Scientifique et Technique Internationale du Vol à Voile) at Buxton, England, 1954.

2. Preliminary theory

In Part I it was shown that the steady-state motion of a stratified fluid in a channel was governed by the equation

$$\nabla^2 y_0 + \frac{1}{2}\left[(\nabla y_0)^2 - 1\right]\frac{d}{dy_0}\ln(U^2\varrho) - \\ - \frac{g}{U^2\varrho}\frac{d\varrho}{dy_0}(y_0 - y) = 0 \qquad (1)$$

where y_0 is the height of a streamline far upstream, and $U(y_0)$, $\varrho(y_0)$ are the velocity and density distributions far upstream. The assumptions in the derivation of this equation are the following:

(1) The fluid is incompressible.

(2) The flow is steady and two-dimensional.

(3) Sufficiently far upstream from the source of disturbance (obstacle), $y_0 = y$ and the velocity and density distributions (U, ϱ) are known functions of the vertical coordinate.

The significance of assumption (3) should be emphasized. In effect it is assumed that the flow and density are initially given by $U(y)$, $\varrho(y)$. An obstacle is then inserted in the stream and a steady state is awaited. It is not only assumed that the flow reaches a steady state but that the velocity and density fields approach $U(y)$ and $\varrho(y)$ if we go sufficiently far upstream. It is conceivable that the obstacle could cause an alteration of the basic distributions U, ϱ to propagate indefinitely far upstream. In this case either the flow would never come to a steady state or else it would approach a new distribution $U'(y)$, $\varrho'(y)$ upstream.

Equation (1) is highly non-linear if $U(y_0)$, $\varrho(y_0)$ are assigned arbitrarily. If, however, we suppose that we deal with a model in which ϱ is linear in y_0 and $U^2\varrho$ = const we obtain the linear equation

$$\nabla^2\delta + \sigma^2\delta = 0, \quad \delta = y - y_0, \quad \sigma^2 = \frac{g}{U^2\varrho}\left|\frac{d\varrho}{dy_0}\right| \qquad (2)$$

In (2), δ represents the variation in height of the streamline y_0 = const about its equilibrium (upstream) height. A model with a linear density gradient is, of course, of considerable interest physically, but it is perhaps unlikely that we will encounter the condition $U^2\varrho$ = constant in practical applications. In geophysical problems involving stratification ϱ varies very slowly with height (the analogous quantity in the atmosphere is potential density). $U^2\varrho$ = const will then imply a very small increase of velocity with height. It may be hoped then that the present model will contain the essential features of a statified fluid with constant density gradient and uniform velocity. This is the viewpoint adopted in this paper; the experiments show that no sensible error results from the approximation.

3. Theoretical flow of a stratified fluid over an obstacle

The solution of equation (2) for flow in an infinite channel with rigid, parallel, upper and lower boundaries is straightforward provided the obstacle at the bottom of the channel is considered to be infinitesimal in height. The solution turns out to be indeterminate if σ exceeds a certain value, but it has long been recognized that this indeterminancy may be removed by introducing viscosity[1] (RAYLEIGH 1883). The simplest possible equation for such motion with damping is

$$\frac{\partial}{\partial x}(\nabla^2\delta' + \sigma^2\delta') = \mu\delta' \qquad (3)$$

The solution of (3) for the same boundary conditions is unique and when μ approaches zero, δ' approaches a solution of (2). The only effect of friction that remains when μ vanishes is the absence of wave motions upstream.

We are, however, interested in flow over an obstacle of finite height and this makes the standard approach by Fourier integrals so complicated that it is practically impossible. Lacking a better method, a finite solution was derived in the following manner: The solution was obtained first for an infinitesimal obstacle of some convenient shape. This solution is of the form

$$\delta = a\,f(x, y; \sigma, b) \qquad (4)$$

where b relates to the length of the barrier and a is the maximum height of the infinitesimal barrier. If in (4) we arbitrarily assign a finite

[1] Recently STOKER (1953) has shown that in the flow of a liquid with free surface, the indeterminancy is also avoided by solving the problem from an initial state, then letting $t \to \infty$.

value to a the resulting solution still satisfies (2) exactly. When the solution is plotted, the material curve $y_0 = 0$ lies on the line forming the bottom of the channel everywhere except in the vicinity of the origin of x, where it rises into the channel, reaching a maximum height and then returning to the line $y = 0$. If we take the $y_0 = 0$ curve as the new channel bottom, (4) represents, in effect, flow of the stratified fluid over a certain obstacle whose height and shape are obtained in the above indirect manner. A disadvantage of this method is that the resulting obstacle is not always symmetric about the line $x = 0$. The asymmetry is usually slight, however, and the height and length of the barrier can be varied by varying a and b.

We assume as the solution of (2) the following:

$$\delta(x \leq -b) = \delta_1 = \sum_{n=n_1+1}^{\infty} A_n e^{a_n x} \sin n\pi y \tag{5}$$

$$\delta(-b \leq x \leq b) = \delta_2 =$$

$$= \sum_{0}^{\infty} E_n \cos \frac{n\pi x}{b} \sin \left(\sigma^2 - \frac{n^2\pi^2}{b^2}\right)^{1/2} (1-y) +$$

$$+ \sum_{n=1}^{n_1} (F_n \cos a_n x + G_n \sin a_n x) \sin n\pi y +$$

$$+ \sum_{n=n_1+1}^{\infty} (H_n e^{a_n x} + M_n e^{-a_n x}) \sin n\pi y \tag{6}$$

$$\delta(x \geq b) = \delta_3 = \sum_{n=1}^{n_1} (B_n \cos a_n x +$$

$$+ C_n \sin a_n x) \sin n\pi y +$$

$$+ \sum_{n=n_1+1}^{\infty} D_n e^{-a_n x} \sin n\pi y \tag{7}$$

In these expressions the height of the channel is taken as 1, and the obstacle has a height $y_s = f(x)$ for $-b \leq x \leq b$, $y_s = 0$ elsewhere. The quantities E_n and a_n are

$$E_n = \frac{1}{b \sin \left(\sigma^2 - \frac{n^2\pi^2}{b^2}\right)^{1/2}} \int_{-b}^{b} f(x) \cos \frac{n\pi x}{b} \, dx, \; n \geq 1$$

$$E_0 = \frac{1}{2\, b \sin \sigma} \int_{-b}^{b} f(x)\, dx, \quad a_n = |\sigma^2 - n^2\pi^2|^{1/2} \tag{8}$$

The integer n_1 is the last for which $(\sigma^2 - n^2\pi^2)$ is a positive quantity. The assumed solution satisfies equation (2) and the kinematic conditions at the top of the channel $y = 1$, at the bottom, $y = 0$ and, with the assumption that $f(x)$ is infinitesimal, the kinematic condition at the obstacle. Moreover, there are no upstream waves. The constants A_n, B_n, C_n, D_n, F_n, G_n, H_n, M_n are available to establish continuity at the lines $x = \pm b$. They are determined by requiring that δ and δ_x be continuous at these lines. Omitting this straightforward procedure, and choosing a special obstacle

$$f(x) = \frac{a}{2}\left(1 + \cos \frac{\pi x}{b}\right), \quad -b \leq x \leq b$$

$$f(x) = 0 \text{ elsewhere} \tag{9}$$

we obtain

$$\delta_1 = -a \sum_{n=n_1+1}^{\infty} \frac{\gamma_n}{2} \left[e^{a_n(x+b)} - e^{a_n(x-b)}\right] \sin n\pi y \tag{10}$$

$$\delta_2 = \frac{a}{2 \sin \sigma} \sin \sigma (1-y) +$$

$$+ \frac{a \cos \frac{\pi x}{b}}{2 \sin \left(\sigma^2 - \frac{\pi^2}{b^2}\right)^{1/2}} \sin \left(\sigma^2 - \frac{\pi^2}{b^2}\right)^{1/2} (1-y) +$$

$$+ a \sum_{n=1}^{n_1} \gamma_n \cos a_n (x+b) \sin n\pi y +$$

$$+ a \sum_{n=n_1+1}^{\infty} \frac{\gamma_n}{2} \left[e^{-a_n(x+b)} + e^{a_n(x-b)}\right] \sin n\pi y \tag{11}$$

$$\delta_3 = -a \sum_{n=1}^{n_1} 2\, \gamma_n \sin a_n b \sin a_n x \sin n\pi y -$$

$$- a \sum_{n=n_1+1}^{\infty} \frac{\gamma_n}{2} \left[e^{a_n(x-b)} - e^{-a_n(x+b)}\right] \sin n\pi y \tag{12}$$

The coefficient γ_n is

$$\gamma_n = \frac{n\pi}{\sigma^2 - n^2\pi^2} - \frac{n\pi}{\sigma^2 - n^2\pi^2 - \frac{\pi^2}{b^2}} \tag{13}$$

The combined solution δ has the following properties:

(a) δ and its first derivatives with respect to x and y exist and are continuous for all x and y in the field of flow, except when $\sigma^2 = p^2\pi^2$, $p = 1, 2 \ldots$.

(b) Second derivatives of δ with respect to x and y ($\sigma^2 \neq p^2\pi^2$) exist for all x and y in the field of flow, except at the points $(b, 0)$, $(-b, 0)$. Equations (10)—(12) represent, therefore, a solution of (2) for flow in an infinite channel over an infinitesimal obstacle (9). The non-existence of the second derivative at the two boundary points is simply an expression of the non-existence of $f''(x)$ at these points. The significance of the exceptional values of σ will be discussed in section 6.

As previously indicated we may assign a finite value to a and obtain thereby the solution for flow over a certain finite obstacle. Since $\delta = y - y_0$, the equation for the obstacle $y = h(x)$ is

$$h(x) - \delta[x, h(x)] = 0 \tag{14}$$

If $\sigma < \pi$ it is easily shown that δ has no nodal lines within the fluid running along the direction of the channel. (POCKELS 1891). Therefore the maximum height of the obstacle varies monotonically, being 1 when $a = \infty$. If $\sigma > \pi$, however, such nodal lines exist[1]. In this range the height of the obstacle approaches the height of the first nodal line above it as $a \to \infty$. Therefore, it is clearly impossible to obtain a steady state flow over an obstacle higher than this. The computations based on equations (10)—(12) indicate that the maximum obstacle may be varied somewhat by varying b, but for any reasonable value of b, including an indefinitely large half width, there is a maximum obstacle height when $\sigma > \pi$.

4. Solution for a very long obstacle

The solution for infinite b is very simple and illuminating. We are then only interested in the solution δ_2 (equation 11), which reduces to

$$\delta = \frac{a \sin \sigma(1-y)}{\sin \sigma} \tag{15}$$

[1] It is apparent from equation (4) that the equation of the nodal curves is independent of a.

If the (nearly) constant height of the barrier is $\beta(x)$,

$$\delta = \beta(x) \frac{\sin \sigma(1-y)}{\sin \sigma(1-\beta)} \tag{16}$$

It may be noted that this is the solution of the partial differential equation

$$\frac{\partial^2 \delta}{\partial y^2} + \sigma^2 \delta = 0 \tag{17}$$

which is derived from (2) by assuming infinitely slow variations of δ in the direction along the channel. This is analogous to the hydrostatic assumption made in Part II. The singularities of this equation are the straight lines in fig. 1. We note again that if $\sigma < \pi$, the height, β, may have any value between 0 and 1. As in the full solution there is a singularity for infinitesimal barriers when $\sigma = p\pi$, $p = 1, 2, 3 \ldots$. Aside from these values of σ there is a maximum barrier for every $\sigma > \pi$ given by the distance from the $\beta = 0$ axis to the first straight, sloping line above it (denoted by $R_i = -\infty$). In general the larger σ the smaller the maximum obstacle.

For the solution (16), and for the full solution, non-existence corresponds to an infinite velocity at some points of the fluid. If the obstacle is near its maximum size we will have very high velocities and therefore very high shears. It is to be expected that this will lead to a breakdown into turbulence so that the solution may exist but be unstable. Moreover, in (16) a high obstacle means a negative velocity ($\sigma > \pi$) at some level and this corresponds in the full solution to closed circulations above or in the lee of the barrier. Since the density is constant on a streamline, such a closed circulation implies, necessarily, local regions in which density *increases* vertically. This may be shown analytically as follows: Since $\varrho = \varrho_0 (1 - ky_0)$,

$$\frac{\partial \varrho}{\partial y} = -k\varrho_0 \frac{\partial y_0}{\partial y} \tag{18}$$

However, the local velocity along the channel is

$$u = -\frac{\partial \psi}{\partial y} = -\frac{d\psi}{dy_0}\frac{\partial y_0}{\partial y} = U \frac{\partial y_0}{\partial y} \tag{19}$$

so that

$$\frac{\partial \varrho}{\partial y} = -k\varrho_0 \frac{u}{U} \tag{20}$$

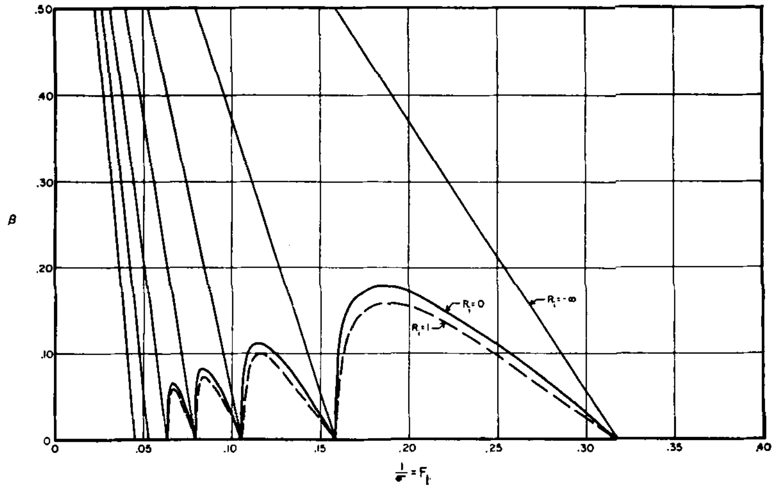

Fig. 1. Graph of solutions for flow over very long obstacle of height β (x). The solid, straight lines ($R_i = -\infty$) represent the singularities of the solution (16). At the given Froude number, the distances from the abscissa to the first line, $R_i = -\infty$, above it is the maximum height of the barrier. The solution does not exist for a higher barrier. If the extreme height of the obstacle is the distance from the abscissa to the solid curve labeled $R_i = 0$, the velocity, u, is just zero somewhere in the fluid above the barrier. For a higher obstacle, closed cells appear and the solution is unstable. If the extreme height of the barrier is the distance to the dashed curve labeled $R_i = 1$, the Richardson number (24) falls to one somewhere in the fluid. For higher barriers $R_i < 1$, and shearing instability may arise.

The density increases with height (overturning instability) if $u < 0$. The exact criterion may be derived from (16):

$$y_0 = y - \frac{\beta \sin \sigma(1-y)}{\sin \sigma(1-\beta)} \tag{21}$$

Differentiating with respect to y, the necessary and sufficient condition for overturning instability is

$$\min \left[1 + \frac{\sigma\beta \cos \sigma(1-y)}{\sin \sigma(1-\beta)} \right] \leq 0 \tag{22}$$

An investigation of (22) shows that the minimum occurs at nodal surfaces of the function $\delta = y - y_0$. If $\sigma < \pi$ the velocity u exceeds U everywhere and can never become negative. Hence *no overturning instability can occur for* $\sigma < \pi$ *regardless of the size of the barrier.*

When $\pi < \sigma < 2\pi$ the minimum occurs at the top of the channel where $y_0 = y = 1$ and this minimum will be negative if

$$1 - \frac{\sigma\beta}{|\sin \sigma(1-\beta)|} < 0 \tag{23}$$

It is easily seen that (23) is the criterion for instability for all $\sigma > \pi$. The inequality (23) corresponds to the area above the curves marked $R_i = 0$ in fig. 1. We note that the lower the Froude number, the smaller the barrier must be to avoid the overturning instability. There is thus a considerable range in which the solution exists but is unstable.

It is possible, of course, that the fluid system may break down for even smaller obstacles than the ones indicated by the curves of (23), due possibly to shearing instability. We have no clear guide for this investigation, although an obvious choice is to plot the maximum obstacle for which the *minimum* Richardson number in the field is just equal to one, i.e. we *assume* for stability that

$$\min R_i \geq 1, \quad R_i = \frac{\dfrac{-g}{\varrho}\dfrac{\partial \varrho}{\partial y}}{\left(\dfrac{\partial u}{\partial y}\right)^2} \tag{24}$$

Since U is practically constant, the Richardson number then becomes

$$R_i = \frac{\sigma^2 \left(\frac{\partial y_0}{\partial y}\right)}{\left(\frac{\partial^2 y_0}{\partial y^2}\right)^2} =$$

$$= \sin \sigma(1-\beta) \frac{[\sin \sigma(1-\beta) + \beta\sigma \cos \sigma(1-y)]}{\beta^2 \sigma^2 \sin^2 \sigma(1-y)} \qquad (25)$$

Furthermore, min $R_i(y) = R_i(y_s)$ where

$$\left(\frac{\partial R_i}{\partial y}\right)_{y_s} = 0, \quad \left(\frac{\partial^2 R_i}{\partial y^2}\right)_{y_s} > 0 \qquad (26)$$

These relationships define y_s by the equation

$$\cos \sigma(1-y_s) = -\frac{1}{\sigma\beta} \sin \sigma(1-\beta) \pm$$
$$\pm \sqrt{\frac{1}{\sigma^2\beta^2} \sin^2 \sigma(1-\beta) - 1} \qquad (27)$$

Since the two terms on the right in (27) must be of opposite signs,

$$\cos \sigma(1-y_s) = -\frac{1}{\sigma\beta} \sin \sigma(1-\beta) +$$
$$+ \frac{\sin \sigma(1-\beta)}{|\sin \sigma(1-\beta)|} \sqrt{\frac{1}{\sigma^2\beta^2} \sin^2 \sigma(1-\beta) - 1} \quad (28)$$

Therefore

$$\min R_i = \frac{|\sin \sigma(1-\beta)| \sqrt{\frac{1}{\sigma^2\beta^2} \sin^2 \sigma(1-\beta) - 1}}{2\sigma\beta \left\{1 - \frac{1}{\sigma^2\beta^2} \sin^2 \sigma(1-\beta) + \frac{|\sin \sigma(1-\beta)|}{\sigma\beta} \sqrt{\frac{1}{\sigma^2\beta^2} \sin^2 \sigma(1-\beta) - 1}\right\}} \qquad (29)$$

Defining

$$x = \frac{\sin \sigma(1-\beta)}{\sigma\beta} \qquad (30)$$

the condition that min $R \geq 1$ is

$$-|x| + 2\sqrt{x^2 - 1} \geq 0 \qquad (31)$$

This is satisfied in the regions below the curves marked $R_i = 1$ in fig. 1. We note that the $R_i = 1$ curves and the $R_i = 0$ curves are quite close, so that for practical purposes either may be chosen as the stability criterion.

5. Discussion of solution for flow over obstacle of finite length and height

Returning to the more important case of barriers of finite length, the problem of obtaining the pattern of flow, and information similar to the above, is one of laborious computation. This has been done for a number of values of σ and b, and for values of a yielding well-developed wave motion. The results are contained in figs. 6—13 in which the theoretical and comparable experimental flow patterns are shown together. In many of the calculated flows the obstacle is so large that closed cells appear. It need only be remembered that smaller values of a will eliminate these cells and yield a somewhat smaller barrier. Otherwise the pattern of flow will be unaffected. A discussion of the most important features o the motion is presented in the next section where a comparison is made with the experiments.

Computations were not performed for very small values of b. Such flow would be over very abrupt obstacles and in actual experiment boundary layer separation effects would dominate, rendering the theoretical solution almost useless.

We may observe from the computations leading to the above figures, and additional computations, the maximum obstacle for existence and for eliminating closed circulations. If the parameter a is given such large values that the obstacle approaches its maximum height for existence, the barrier obtained is very asymmetric, rising sharply on the upwind side and dropping very rapidly on the lee. The calculations were restricted then to obtaining the maximum obstacle for overturning stability (no closed circulations). The results are presented in fig. 2. They are analogous to the curves marked $R_i = 0$ in fig. 1. We note that the latter, based on the assumption of an infinitely long barrier, are very similar and provide a close approximation. Except near the singular values of the Froude number, the

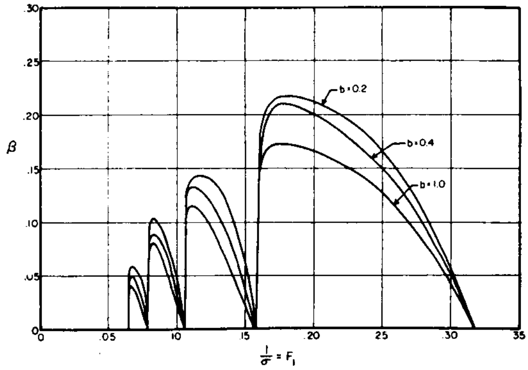

Fig. 2. Maximum obstacle heights for overturning instability in flow over a barrier of half length .2, .4, 1.0. The three curves give the maximum height of the barrier at a given Froude number. Higher obstacles will be associated with the appearance of turbulence at some points of the fluid. Smaller barriers will have laminar flow over them.

curves indicate, roughly, $\beta \cong F_i$ when overturning instability begins.

6. Experiments with a stratified fluid

The fact that the solutions in section 5 satisfy the frictionless equations of motion exactly, eliminates one of the major deficiencies of prior investigations of such systems, namely the assumption of infinitesimal obstacle heights. On the other hand, the basic velocity and density distributions $U^2\varrho$ = const, ϱ linear, are not likely to be encountered in natural phenomena or experiment and the practical question arises as to the applicability to real systems in which the distributions of velocity and density are only approximations to these relationships. One system which can be produced experimentally is a basic velocity distribution U = const and ϱ nearly linear and very slowly decreasing with height. In such a case the σ of equation (2) is nearly constant and any other terms that enter the complete equation (1) are small compared to the terms of (2). This type of system was investigated and a comparison made below between experimental results and the theory of section 3.

The physical set up is a long channel (fig. 3) containing a mixture of water and salt with a smooth density-height curve. An obstacle is towed by a motor drive at a constant speed along the bottom. The percentage density gradient from top to bottom is small (10 per

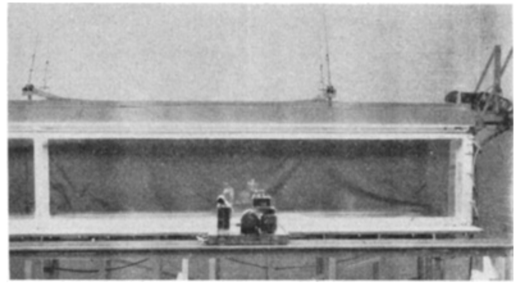

Fig. 3. Channel used for stratified fluid experiments. The entire channel is 20 ft long, 6 in wide and 2.5 ft high.

cent or less). The density-height curve is roughly linear except at the top and bottom of the channel where the fluid tends to have a uniform concentration of salt. Using the speed of the barrier, the depth of the water and a representative density difference, we may compute for each experiment a Froude number

$$F_i = \frac{U}{\left(g \dfrac{\Delta \varrho}{\varrho} H\right)^{1/2}}$$

which is of the form of $1/\sigma$ in equation (2).

Considerable question arises regarding the computed Froude number of the experiments. The uncertainty is in the value of $\Delta\varrho/\varrho$. If the density gradients in the experiment were linear this would be simply the measured difference in density from top to bottom divided by the mean density. Actually the density gradients resemble that shown in fig. 4. As mentioned earlier, there is a considerable tendency to have a homogeneous layer at top and bottom. An explanation for this was suggested to the writer

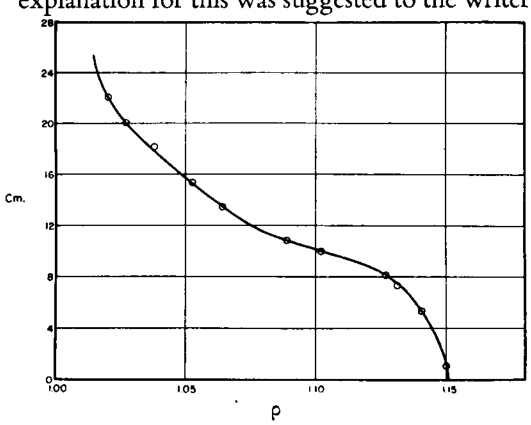

Fig. 4. Density-height curve for fig. 5.

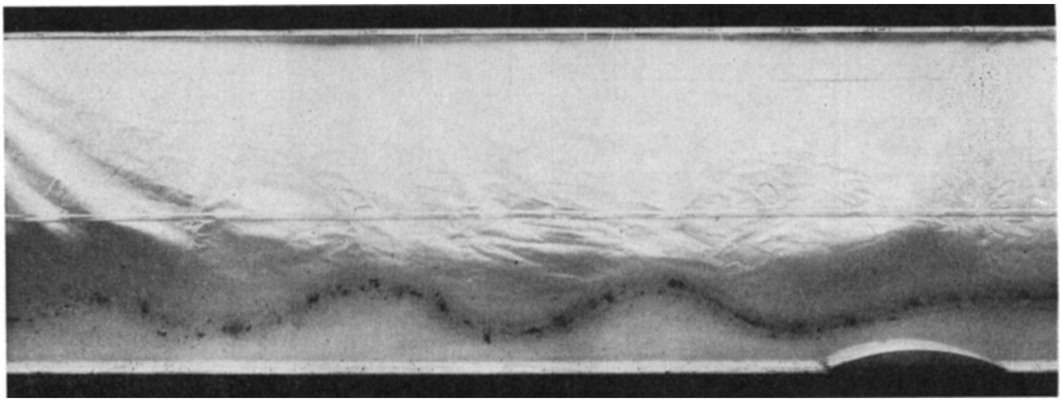

Fig. 5. Sine waves in flow over barrier. F_i = .220, β = .137, b = .59. The length of the waves is approximately 1.90.

by Sir Geoffrey Taylor, who remarked that if the mixing of the salt by turbulent diffusion be regarded as Fickian diffusion, the absence of flux of salt through the bottom and top surfaces would require the vanishing of the normal derivative of salt concentration, and a tendency for homogeneous layers at top and bottom.

The observed density distribution offers two possibilities for computing $\Delta\varrho$: the difference in density at top and bottom, or the $\Delta\varrho$ obtained by extrapolating the mean slope of the curve in the interior of the fluid. The flow pattern associated with the density curve in fig. 4 suggests an answer. Fig. 5 is the photograph of this flow. If $\Delta\varrho$ is taken as the density difference from top to bottom, the computed Froude number is .253; using the average gradient in the interior we obtain .220. Since the theoretical wave length is

$$\lambda = \frac{2\pi}{(F_i^{-2} - \pi^2)^{1/2}}$$

we obtain λ = 2.64, 1.94 respectively. Since the measured length is 1.90 (approximately), the fluid system seems to behave as if it had a linear density gradient equal to the average slope of the density curve in the interior. Because of this, the computed values of F_i in this paper are based on slope of the density curve in the interior of the fluid. It is perhaps of some importance meteorologically that a lower homogeneous layer (adiabatic layer) has no sensible effect on the phenomena.

The obstacles used in the experiments are of various sizes but all have an "easy shape" to reduce the effects of boundary layer separation. The ratio (β) of maximum obstacle height to the total depth is varied by using different obstacles and different fluid depths (H). Observations are made by recording the motion of aluminum tracer particles by a time exposure on a photographic plate. The camera is moved on a track at the speed of the obstacle so that the recorded flow is approximately steady.

The main features of the experiment are revealed in figs. 6—13 in which the flows are shown in the order of decreasing Froude number. Fig. 6 is flow at a very high speed. The motion involves only a symmetrical elevation of the streamlines over the barrier. Experimentally it resembles potential flow very closely. Theoretically, it is obvious that the density gradient generates some negative vorticity as the fluid rises over the barrier. This eliminates the need for the strong decrease of velocity with height that accompanies potential flow. As a result the vertical velocities extend to greater heights and the horizontal component increases by about the same amount at all levels. For purposes of comparison with the atmosphere we note that if we relate the total depth of fluid to the height of the tropopause, the Froude number of .350 corresponds to a mean velocity of 45 m/sec. The theoretical flow is for a somewhat higher Froude number but since both are above the critical number π^{-1} they are very similar.

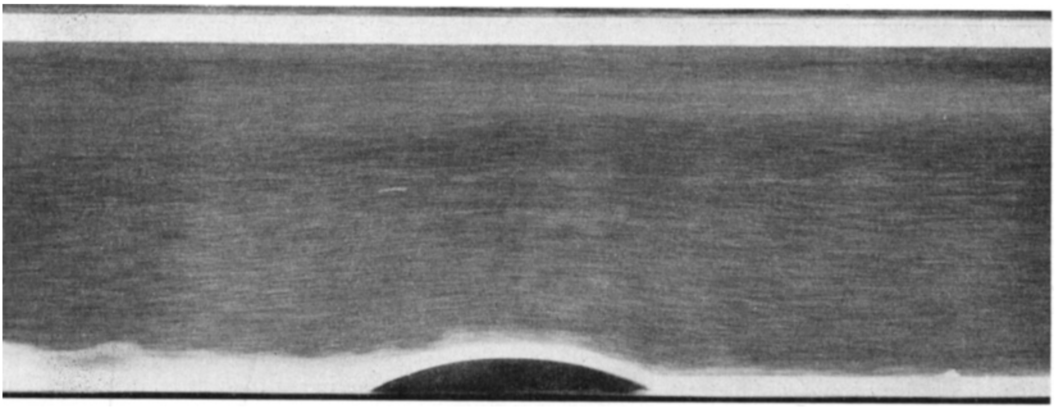

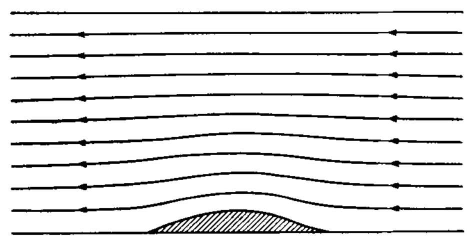

Fig. 6. Observed and calculated flow over an obstacle. Theoretical: $F_i = .500$, $\beta = .100$, $b = .4$, $a = .14$. Experimental: $F_i = .350$, $\beta = .092$, $b = .42$.

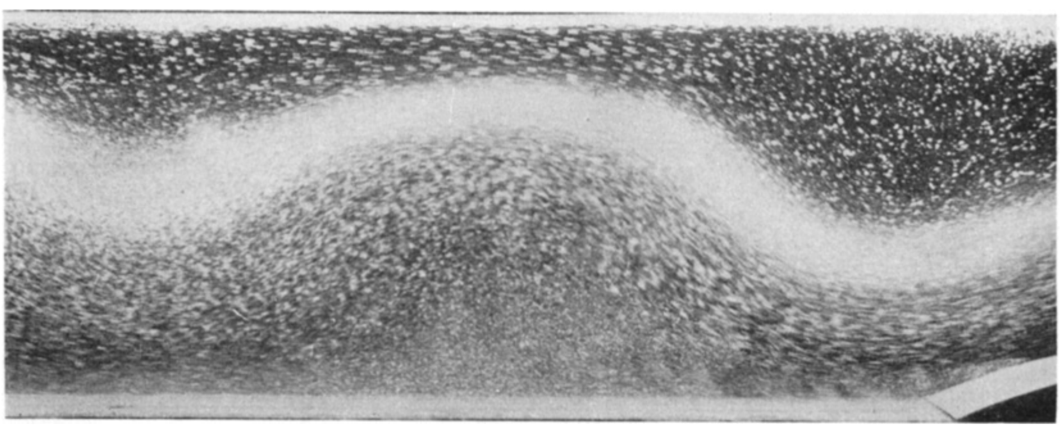

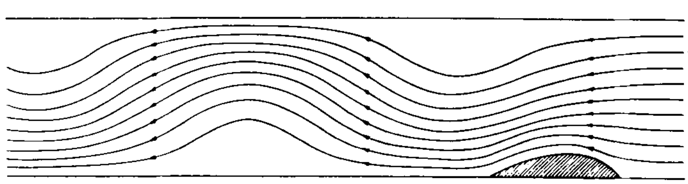

Fig. 7. Observed and calculated flow over an obstacle. Theoretical: $F_i = .250$, $\beta = .150$, $b = .4$, $a = .30$. Experimental: $F_i = .233$, $\beta = .151$, $b = .57$.

Fig. 7 shows a flow pattern at a Froude number in the range $(2\pi)^{-1} < F < \pi^{-1}$. A long wave appears in the lee. The theoretical wave length, at the F_i of the experiment (somewhat smaller than the F_i of the drawing), is 2.1 H, which is very close to the observed length. According to fig. 2 the β of the experiment is just below the value calling for zero horizontal velocities at some places in the field. We see in the photograph that a large region in the upper part of the channel just in thelee contains fluid at rest with respect to the barrier. There is no evidence of turbulence in this region; we would anticipate its onset for a somewhat larger value of β. The turbulence appearing near the bottom under the first crest of the wave is not due primarily to overturning or shearing instability but to boundary layer separation. In all experiments this effect tends to cause turbulence beneath the first crest in the lee. This is to be expected because this area corresponds to a minimum of velocity and therefore a maximum of dynamic pressure. The resulting adverse pressure gradient just upstream will cause separation. The fluid in the boundary layer is then carried into the body of the fluid to form a large turbulent eddy.

Fig. 8 is another example of flow in the range of a single sine wave in the lee. The obstacle is quite large; the waves have developed beyond the point of overturning instability. This is shown by the appearance of turbulence in the reversal region at the free surface just in the lee. This, and the turbulence below the first crest (due partly to boundary layer separation and partly to overturning instability), has removed so much energy that the waves further downstream are greatly weakened. The size of the obstacle is such that a theoretical solution exists although it is unstable. We see, nevertheless, that the obstacle is causing a blocking action upstream. This is evidenced by the shortness of the streaks in the fluid near the bottom ahead of the barrier. We have in this an indication that an alteration of upstream density and velocity distribution takes place in the range where a steady-state solution exists but is unstable.

Fig. 9 is flow below the second critical number, $F_i = 1/2\pi$. As shown in both theory and experiment the streamlines tend to open up in the region midway between top and bottom and just in the lee. At the F_i of the experiment fig. 2 indicates a reversal of velocity above a β of .075. Since the β of the experiment is well above this we have definite, turbulent eddies. The resultant loss of energy prevents the appearance of a second eddy downstream as predicted by the theoretical drawing, although there is evidence of a velocity reduction in the appropriate region downstream.

Fig. 10 represents a further reduction in F_i to the range $(4\pi)^{-1} < F_i < (3\pi)^{-1}$, and shows a remarkable array of eddies downstream, whose positions and distances correspond very closely to those in the theoretical drawing. The discrepancy in the two Froude numbers leads only to a shortening of wave length in the observed flow. Fig. 2 indicates a β of .087 for overturning instability at the F_i of .084. This is verified by the experiment, since the eddies appear slightly turbulent but not enough to prevent repetitions of the pattern downstream. It is interesting to note that the "S"-shaped streamlines above the barrier appear in both theory and experiment.

Fig. 11 is another example of flow in the range $(4\pi)^{-1} < F_i < (3\pi)^{-1}$. The obstacle is very large and the flow is therefore very turbulent. An outstanding feature is the exaggerated crest in the lee where the flow is strongly affected by boundary layer separation. In other respects the experiment and theory agree closely.

Fig. 12 is an example of flow in the range $(5\pi)^{-1} \leq F_i < (4\pi)^{-1}$. The theoretical flow is for a Froude number very close to the critical value $(4\pi)^{-1}$. The result is a well-developed wave motion for a very small barrier. The observed flow is at a Froude number corresponding to a β of .048 in fig. 2. Since the β in the experiment is .056 we would expect the definite turbulence in the eddies seen in the photograph. Moreover the tendency for blocking the lower fluid ahead of the barrier is very evident. The eddies just in the lee appear in the same position in the theoretical and experimental flows, and the other details correspond very closely.

Little effort was made to investigate the singular points of the theoretical solution in sections 4 and 5, i. e., the values of $\sigma = p\pi$. These singularities are expressions of the fact that a long wave of undetermined amplitude can exist at those values of σ in a channel with

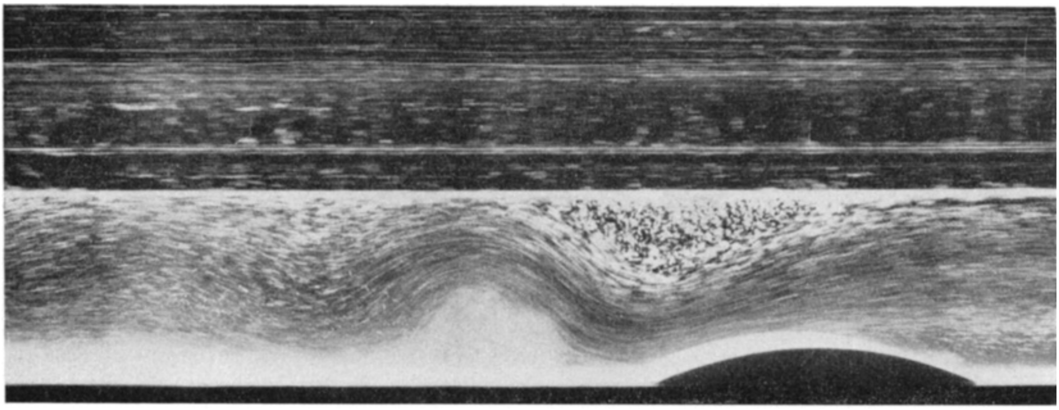

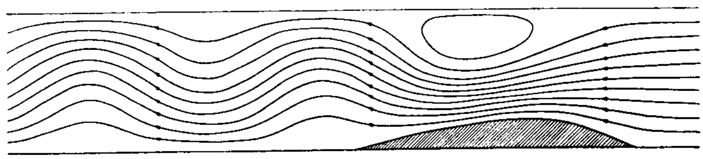

Fig. 8. Observed and calculated flow over an obstacle. Theoretical: $F_i = .200$, $\beta = .200$, $b = 1.0$, $a = .35$. Experimental: $F_i = .204$, $\beta = .200$, $b = .86$.

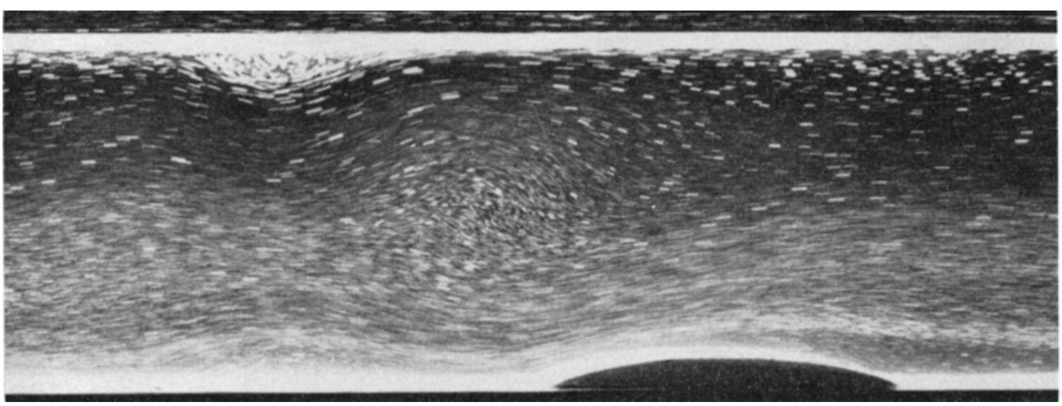

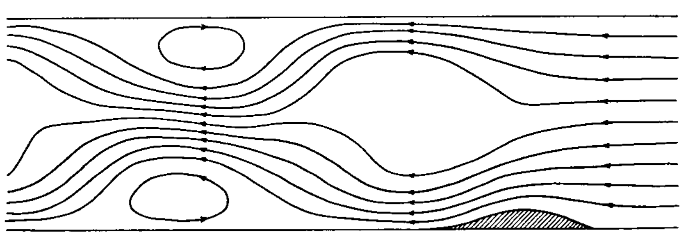

Fig. 9. Observed and calculated flow over an obstacle. Theoretical: $F_i = .143$, $\beta = .100$, $b = .4$, $a = .18$. Experimental: $F_i = .131$, $\beta = .085$, $b = .50$.

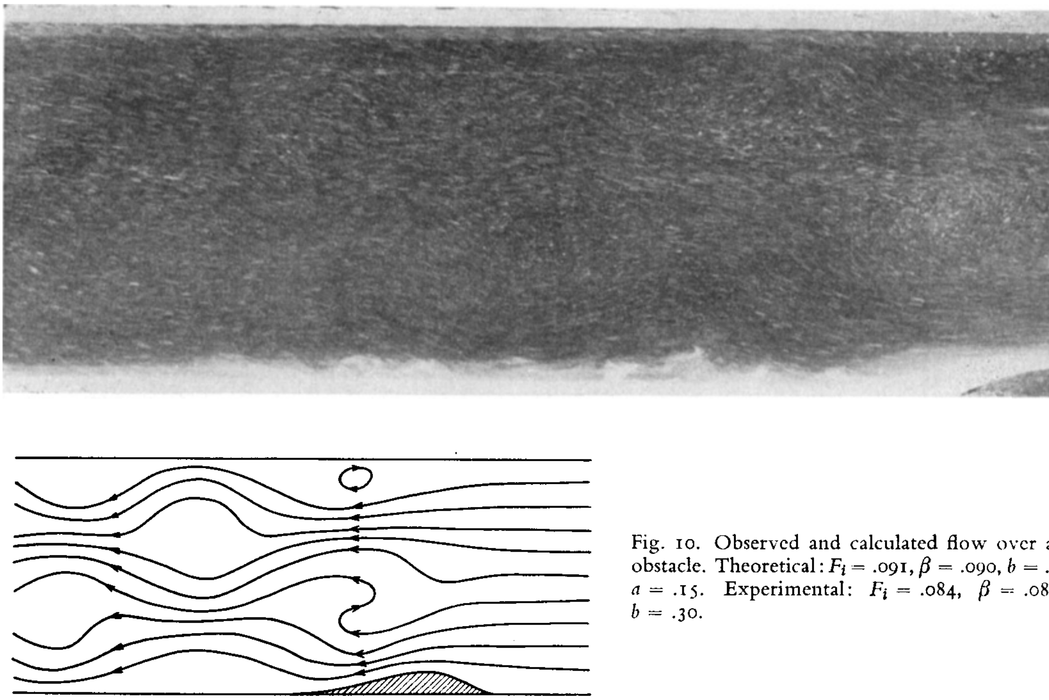

Fig. 10. Observed and calculated flow over an obstacle. Theoretical: $F_i = .091$, $\beta = .090$, $b = .4$, $a = .15$. Experimental: $F_i = .084$, $\beta = .085$, $b = .30$.

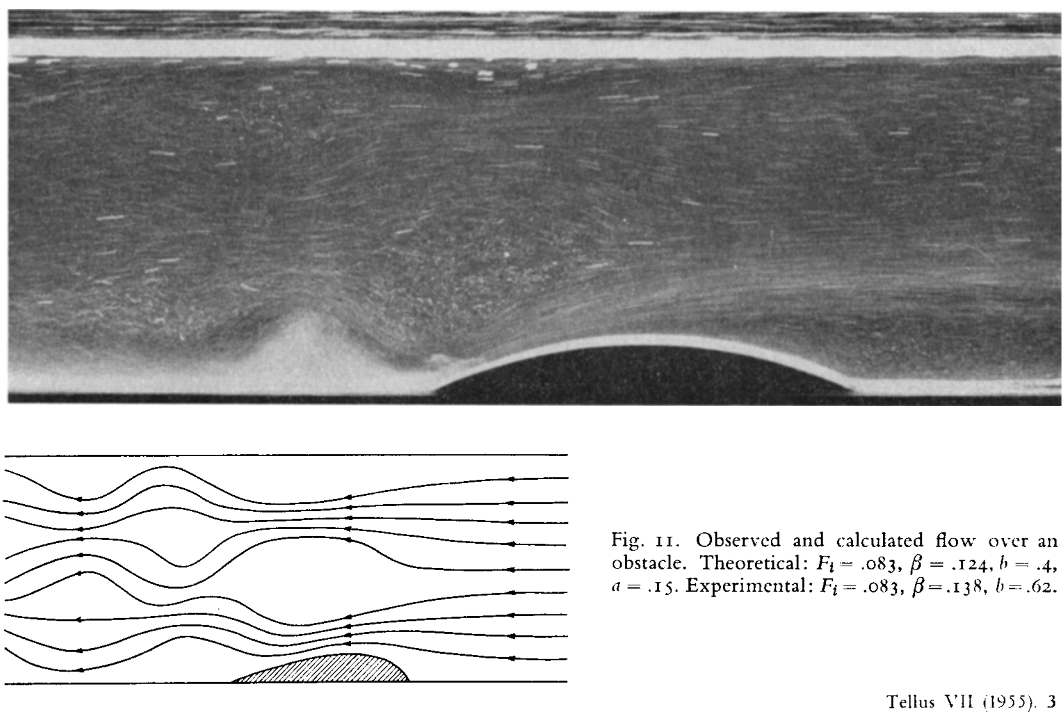

Fig. 11. Observed and calculated flow over an obstacle. Theoretical: $F_i = .083$, $\beta = .124$, $b = .4$, $a = .15$. Experimental: $F_i = .083$, $\beta = .138$, $b = .62$.

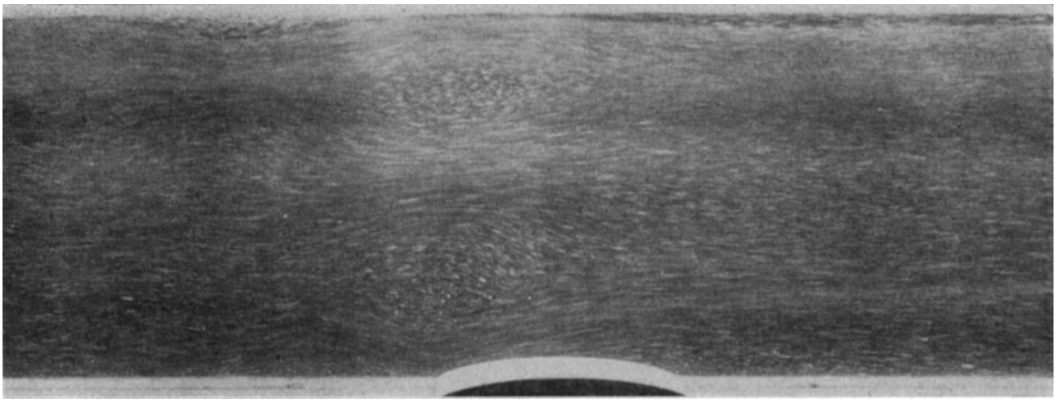

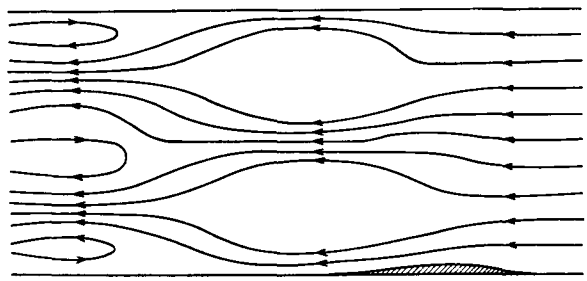

Fig. 12. Observed and calculated flow over an obstacle. Theoretical: $F_i = .077$, $\beta = .030$, $b = .4$, $a = .06$. Experimental: $F_i = .070$, $\beta = .056$, $b = .33$.

plane top and bottom. The same phenomenon occurs in the flow of water with a free surface over an obstacle at the critical Froude number $F^2 = U^2/gH = 1$. The singularity is removed by introducing friction as in equation (3) but the flow patterns remain exaggerated at $\sigma = p\pi$ unless the frictional coefficient is large.

It appears to be impossible to seek for these singularities in the experiment for several reasons: The foremost is the uncertainty in the calculated Froude number. The range of uncertainty is at least as large as the range of σ, on either side of $p\pi$, in which exaggerated wave patterns are indicated for small obstacles. Secondly, the experimental model has distributions of density and velocity upstream which differ from the theoretical model, and if the same kind of singularities exist for the actual conditions of the experiment, they will doubtless occur at Froude numbers sensibly different from $(p\pi)^{-1}$. Thirdly, the time period, from the beginning of the experiment until the recording of the motion by visual or photographic means, is finite and the corresponding time dependent solution may not possess any singularities. Finally it is likely that slight adjustments of the upstream velocity and density fields by blocking effects or other wave propagations upstream will be able to change the "Froude" number to a non-singular value. Such adjustments may not be observable.

An effort was made to investigate the singular value $\sigma = \pi$ by taking a number of photographs in a small range about this value. In this case the quasi-unsteady nature of the experiment made the effort unsuccessful. When σ was slightly less than π, a wave formed in the lee which simply became longer and longer as the experiment progressed. Presumably, it could be made arbitrarily long, and of vanishingly small amplitude, if a channel of very great length were available. Another investigation at values of σ near 2π simply indicated a gradual transition from a simple sine wave pattern for $\sigma < 2\pi$ to the more complex double wave system for $\sigma > 2\pi$.

7. Other experimental results

When the obstacle is very large, in the sense that the solutions of section 3 either do not exist or are unstable, the experiments tend to

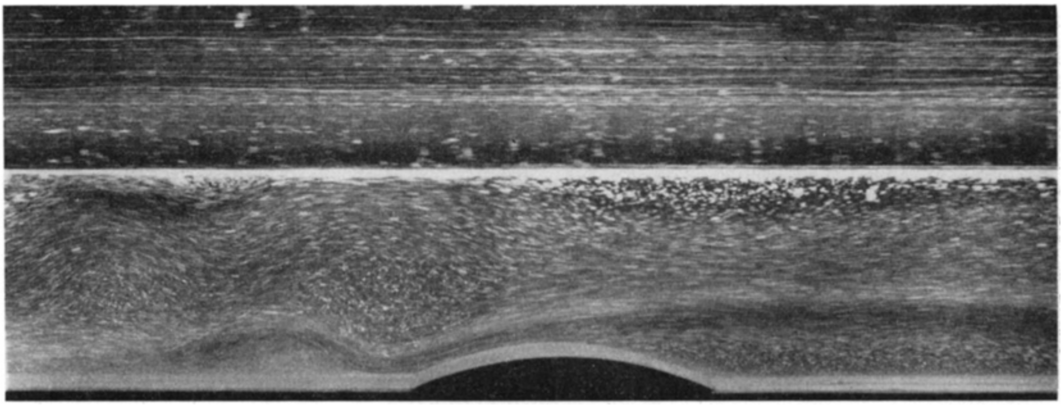

Fig. 13. Jet formation ahead of a large barrier. $F_i = .141$, $\beta = .165$, $b = .71$. Note the stagnation of fluid at top and bottom with jet in between.

indicate that a stable steady-state solution cannot be obtained theoretically even if we drop the assumption of unaffected flow far upstream or include viscosity. As the obstacle is raised in height impulses are sent upstream which lead to alternate jets and stagnation regions in the vertical (fig. 14). At the same time turbulence sets in over the obstacle and in the lee and this persists, at least down to very low Froude numbers. Obviously, this is not a steady state since turbulent fluctuations of velocity are, by their nature, non-steady. It thus appears hopeless to improve on the solution obtained in this paper either by dropping some of the assumptions or by including viscous terms. It is conceivable, of course, that a solution could be obtained as an initial value problem and that it should reveal developments for short time intervals from the initial instant. It is scarcely to be hoped, however, that a solution with viscosity included, is within the realm of possibility even using present high speed electronic equipment. This follows from the fact that the turbulence appears to set in as a large eddy (involving, initially, locally unstable density gradients) and then breaks down rapidly into smaller and smaller cells which would soon become smaller than the distance between grid points in any numerical integration.

It would be well, however, to examine the tendency for jet formation more closely. The fact that jets form and seem to move far upstream is of great importance to meteorology and oceanography. Experiments with homogeneous rotating fluids (LONG 1954) indicate that rotation also favors jet formation so that it is likely that atmospheric and oceanic jet streams are due to these two effects. While this is not a new idea (ROSSBY 1951), it is not known just how rotational and gravitational stability work in creating these velocity maxima. Since the experiments show that the presence of gravitational stability alone is sufficient, it may be argued that a detailed understanding of this simpler phenomenon is a prerequisite for a physical understanding of atmospheric jets.

Such a detailed study has not been made for the purposes of this paper. We may note, however, that a Froude number of less than $1/\pi$ is a necessary requirement, and that the jets become more numerous as F_i is decreased. Fig. 13 is an example of a single jet, forming upstream in the interior of the fluid. The value of (.165) is considerably larger than the maximum for stability at this Froude number. Pronounced eddies therefore are formed in the lee. At the same time the large obstacle blocks the flow of fluid ahead of it both at the bottom and top; to preserve continuity the fluid speeds up in the interior forming a jet. For lower Froude numbers the jets increase in number; as many as 8 or 10 may be seen visually at values of F_i around .01. The ones in the upper part of the fluid are usually weak in such a case and not easily recorded by streak photography. Fig. 14, however, gives some indica-

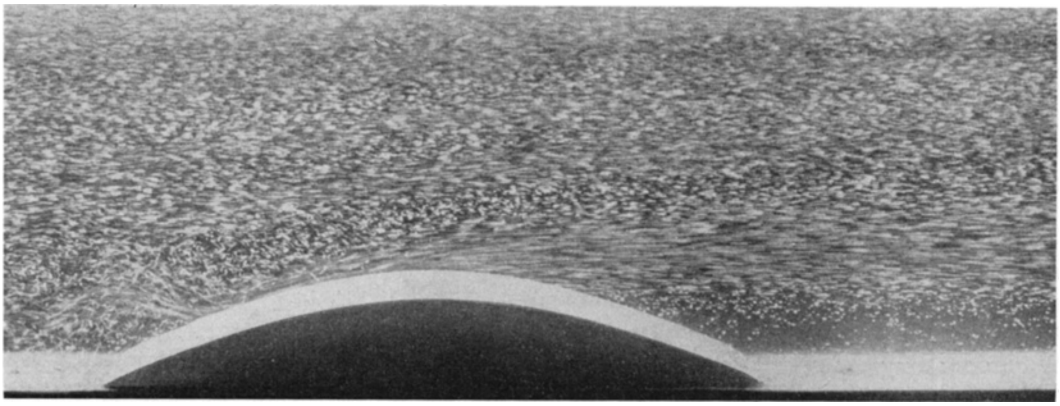

Fig. 14. Multiple jets ahead of the large barrier. $F_i = .017$, $\beta = .150$, $b = .56$. Note the complete blocking of the lowest layer of fluid and sharp velocity shear between this layer and the jet above it.

tion: four jets are visible just over the obstacle, in a depth of about .4 H. All but the lowest one weaken upstream. In many cases the jet nearest the bottom can be seen very easily at distances of 10 H ahead of the barrier, terminating at the end of the channel. The discontinuity of velocity at the bottom of the jet in fig. 14 is extremely sharp. Using the density gradient from top to bottom a local value of the Richardson number at the lower edge of the jet was computed. It is a maximum of .34, and probably smaller, yet no turbulence has appeared in the photograph. However, it is certain that the formation of the jet was accompanied by a very considerably intensification of the density gradient by vertical stretching in the lowest layer of fluid and vertical shrinking in the jet. It is likely that this has increased the Richardson number to a value above 1.0, permitting stability. Thus, the very process by which jets are formed in a stratified fluid presents an agency for their maintenance against turbulent dissipation.

The experiments shed considerable light on the behavior of stratified fluids with other than linear density gradients. If the gradient is confined to a discontinuity or near discontinuity of density across an interface, the phenomena may be expected to be those discussed in Part II, i. e., hydraulic jumps or shock waves in the lee at the interface. In the experiments of this paper the density gradients are obtained by putting first a layer of fresh water in the channel. Another layer of salt water is then inserted at the bottom. Initially a very sharp discontinuity of density exists in the interior. This is destroyed by repeated motions of an obstacle along the bottom. The first run reveals the same phenomena encountered in the flow of two immiscible layers: subcritical motion with little or no disturbance at low Froude numbers, followed by hydraulic jumps at the interface and finally supercritical flow at high Froude numbers. After a few more runs the wave motions typical of continuous gradients begin to appear; the hydraulic jump begins to take on the appearance of the turbulent reversal areas observed in the cases of "linear" gradients. The transition is quite clear if the obstacle is kept at a speed appropriate to the Froude number (.14) of fig. 9. The hydraulic jump develops continuously into the single large eddy in this photograph just downstream in the interior of the fluid. At the same time the more laminar wave motions of fig. 9 begin to appear.

An accompanying theory of non-linear density gradients is necessarily incomplete. If a near-discontinuity of density exists the theory of Part II is available to predict and explain the major features. If the slope of the density curve is smooth the experiments of this paper suggest that the gradient may be considered linear with little error. An intermediate situation involving a general gradient interrupted by one or more inversions (near-discontinuities) is a common one in the atmosphere. Such a model is still governed by equation (2), if we

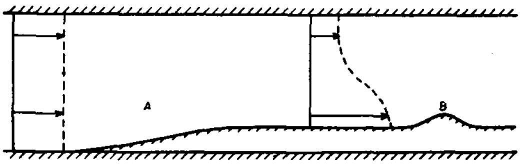

Fig. 15. Obstacle in channel yielding new basic current.

assume a steady state, but this equation is now highly non-linear and intractable. The experiments suggest that the shock-wave phenomenon will dominate if the inversions are very strong, the phenomena of this paper if they are weak.

8. Stratified model with shear and non-linear density gradient

We conclude this paper with a brief discussion of a more general model of a stratified fluid: one that possesses a certain shear of velocity with height in the basic current. In section 4 the solution (16) is valid for the motion of the stratified fluid in a channel whose bottom rises (or falls) very gradually at A in fig. 15, from $y = 0$ to $y = \beta = \text{const.}$ The streamlines and density surfaces will become parallel to the new bottom, but with a velocity and density distribution which we may compute from (16). If, further downstream at B, we disturb the new current in some way, say by inserting an obstacle of finite dimensions, equation (2) will still hold if δ is the variation of the streamline about its old equilibrium height, say y_{00}. However,

$$y_{00} = y_0 - \frac{\beta \sin \sigma (1 - y_0)}{\sin \sigma (1 - \beta)} \qquad (32)$$

where y_0 is now the equilibrium height of the streamline above $y = 0$, upstream of the barrier B but well downstream of A.

This concept leads to another model of a stratified fluid for which equation (1) is linear: In terms of the usual notations of this paper, if we specify a velocity and density distribution in a channel between $y = 0$ and $y = 1$ as

$$U^2 \varrho = \alpha \left[1 + A \cos \sigma y_0 + B \sin \sigma y_0\right]^2 \qquad (33)$$

$$\frac{d\varrho}{dy_0} = \frac{-\sigma^2 \alpha}{g} \left[1 + A \cos \sigma y_0 + B \sin \sigma y_0\right] \qquad (34)$$

we find that equation (1) reduces to

$$(\nabla^2 + \sigma^2)\left(y_0 - y + \frac{A}{\sigma} \sin \sigma y_0 - \frac{B}{\sigma} \cos \sigma y_0\right) = 0 \qquad (35)$$

In this model (which includes $U^2 \varrho = \text{const.}$, ϱ linear as a special case), α, A, B, σ may be varied to obtain currents with various shears of wind with height and density gradients. For example, in the range of $2\pi > \sigma > \pi$, an obvious choice of A and B yields a basic current that is a maximum at the top of the channel and decreases to a minimum somewhere near the bottom. The accompanying density distribution is one of high stability in the upper part of the channel and low stability in the region of weak velocities. Evidently we must require that the velocity in the basic current be of one sign if we are to avoid regions of unstable density gradient. We note also that the disturbed configuration of the streamlines is independent of α.

Equation (35) may be solved for flow over a given obstacle in the manner of section 3. In addition the model may be produced experimentally by use of a long obstacle resembling that in fig. 15. Both the theoretical and experimental investigations are major undertakings and are outside the scope of this paper.

Acknowledgments

The author wishes to acknowledge the help of Mr. James F. Haubert in performing the experimental phases of this research. He was assisted by Messrs. Rudolf Kuster and Harry Mottek. The computations leading to the theoretical flow pattern were performed by Mr. William H. Adams.

REFERENCES

ABDULLAH, A. J., 1954: A proposed mechanism for the development of the eye of a hurricane. *J. of Meteor.* **11**, 189—195.

LONG, R. R., 1953: Some aspects of the flow of stratified fluids. I. A theoretical investigation. *Tellus* **5**, 42—58.

— 1954: Some aspects of the flow of stratified fluids. II. Experiments with a two-fluid system. *Tellus* **6**, 97—115.

— 1954: The motion of an obstacle along the axis of a rotating fluid. Technical Report No. 6, Contract N-onr-248(31).

POCKELS, F., 1891: Über die partielle Differentialgleichung $\triangle u + k^2 u = 0$, Teubner, Leipzig, 339 pp.

ROSSBY, C.-G., 1951: On the vertical and horizontal concentration of momentum in air and ocean currents. *Tellus* **3**, 15—27.

STOKER, J. J., 1953: Unsteady waves on a running stream. *Communications on Pure and Applied Mathematics* **6**, 471—481.

TEPPER, M., 1952: The application of the hydraulic analogy to certain atmospheric flow problems. *W. B. Research paper No. 35*, 50 pp.